

Wind-induced dynamic response and its load estimation for structural frames of circular flat roofs with long spans

Yasushi Uematsu[†]

Department of Architecture and Building Science, Tohoku University, Sendai, Japan

Motohiko Yamada[‡]

New Industry Creation Hatchery Center, Tohoku University, Sendai, Japan

Abstract. This paper describes a simple method for evaluating the design wind loads for the structural frames of circular flat roofs with long spans. The dynamic response of several roof models were numerically analyzed in the time domain as well as in the frequency domain by using wind pressure data obtained from a wind tunnel experiment. The instantaneous displacement and bending moment of the roof were computed, and the maximum load effects were evaluated. The results indicate that the wind-induced oscillation of the roof is generally dominated by the first mode and the gust effect factor approach can be applied to the evaluation of the maximum load effects. That is, the design wind load can be represented by the time-averaged wind pressure multiplied by the gust effect factor for the first mode. Based on the experimental results for the first modal force, an empirical formula for the gust effect factor is provided as a function of the geometric and structural parameters of the roof and the turbulence intensity of the approach flow. The equivalent design pressure coefficients, which reproduce the maximum load effects, are also discussed. A simplified model of the pressure coefficient distribution is presented.

Key words: circular flat roof; wind-induced response; structural frame; load estimation; design wind load; gust effect factor.

1. Introduction

In the structural design of flat long-span roofs, the wind-induced dynamic response should be considered appropriately. Several investigations have been made of the design wind loads for the structural frames of rectangular flat roofs. For example, the gust effect factor (or gust loading factor) for the simple beams supporting flat roofs was studied by Marukawa *et al.* (1993), Ueda and Tamura (1994) and Uematsu *et al.* (1997a); this type of roof is referred to as 'Beam type', in this paper. Uematsu *et al.* (1997b) discussed the gust effect factor for a structurally integrated type of flat roof (referred to as 'Plate type', hereafter), which acts like an elastic plate under wind loading. Regarding circular flat roofs, which are also of Plate type, few studies have been made to date.

This paper discusses the design wind loads for structural frames of circular flat roofs with long

[†] Associate Professor

[‡] Professor

spans. First, we make a dynamic response analysis in the time domain for several roof models, using the wind pressure data obtained from a series of wind tunnel experiments; in the experiments wind pressures are measured simultaneously at some hundred points on the roof. We compute the instantaneous displacement and bending moment of the roof. Based on the results, we discuss the application of a gust effect factor approach to the evaluation of the maximum load effects. Then, another series of wind tunnel experiments is carried out to obtain data for the first modal force under various conditions. Based on the results, we provide an empirical formula for the gust effect factor as a function of the geometric and structural parameters of the roof and the turbulence intensity of the approach flow. Finally, we discuss the equivalent design pressure coefficient, which reproduces the maximum load effects together with the gust effect factor. A simplified model of the pressure coefficient distribution is presented. The application of the empirical formulas obtained in this study is also examined.

It should be mentioned that this paper is an extended version of our previous papers (Uematsu *et al.* 1998 and Sasaki *et al.* 1999).

2. Model roofs and their structural properties

From the structural point of view, the roof behavior under wind loading is represented by that of a thin elastic plate simply supported on the edge. The bending rigidity D_b of the roof is determined so that the maximum deflection of the roof due to the dead load, assumed 980 N/m^2 , becomes $1/300$ of the span D . The variation of the first natural frequency f_1 with span D is shown in Fig. 1. For the purpose of comparison, the results for a Beam type roof and a square roof of Plate type are also plotted; regarding the details, see Uematsu *et al.* (1996, 1997a, 1997b). The value of f_1 varies from approximately 1.5 to

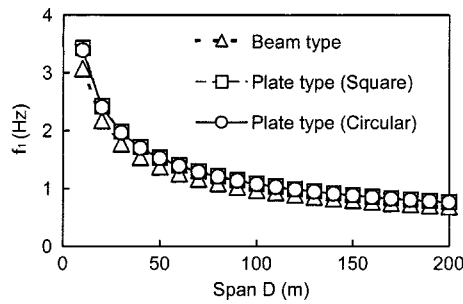


Fig. 1 Variation of the first natural frequency f_1 with span D

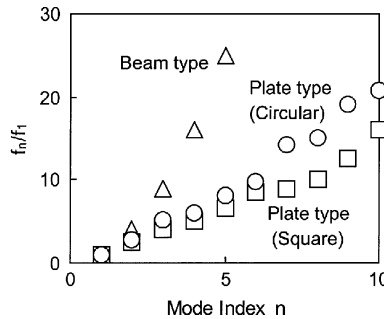


Fig. 2 Ratios of the natural frequencies f_n ($n = 1-10$) to f_1

0.9 Hz, as the span increases from 50 to 150 m. The value slightly depends on the roof type.

The ratio of the natural frequency f_n ($n = 1-10$) to the first mode value f_1 is plotted against the mode index n in Fig. 2; again, the results for a Beam type roof and a square roof of Plate type are included in the figure. In general, the natural frequencies of higher modes are rather high compared with f_1 . For example, the natural frequency of the second mode is approximately three times as high as f_1 for circular roofs. Fig. 3 schematically illustrates the vibration modes for $n = 2-9$. The mode shape becomes more complicated with an increase in n . Table 1 summarizes the numbers (l, m) of nodal circles (the boundary, exclusive) and nodal diameters, which represent the mode shape $\phi_n(r, \theta)$ of vibration,

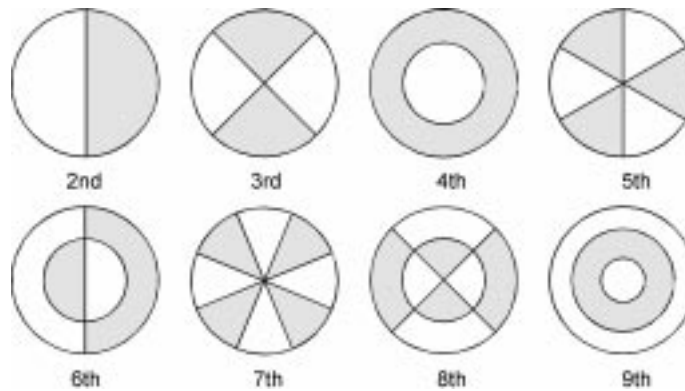


Fig. 3 Schematic illustration of vibration modes $\phi_n(r, \theta)$

Table 1 The numbers (l, m) of nodal circles (the boundary, exclusive) and nodal diameters for the circular roof, which represent the mode shape of vibration

Mode index n for Figs. 2 and 3	Mode index k for Fig. 5	l, m	Mode shape*
1	1	0, 0	Axisymmetric
2	2	0, 1	Asymmetric (S)
	3	0, 1	" (A)
3	4	0, 2	" (S)
	5	0, 2	" (A)
4	6	1, 0	Axisymmetric
5	7	0, 3	Asymmetric (S)
	8	0, 3	" (A)
6	9	1, 1	" (S)
	10	1, 1	" (A)
7	11	0, 4	" (S)
	12	0, 4	" (A)
8	13	1, 2	" (S)
	14	1, 2	" (A)
9	15	2, 0	Axisymmetric
10	16	0, 5	Asymmetric (S)
	17	0, 5	" (A)
11	18	1, 3	" (S)
	19	1, 3	" (A)

*Remarks:

S: mode shape is symmetric with respect to the diameter parallel to the wind direction

A: mode shape is anti-symmetric with respect to the diameter parallel to the wind direction

with (r, θ) being the polar coordinate. The mode shapes for $n = 1, 4$ and 9 are axisymmetric.

3. Experimental arrangements and procedures

Two kinds of wind tunnel experiments were carried out. The experimental conditions are summarized in Table 2. The first series of wind tunnel experiments (series 'A') was carried out in a closed-circuit-type wind tunnel with a working section 2.5 m wide, 2.0 m high and 18.1 m long at Kajima Technical Research Institute. Wind pressures at 433 points on the roof of a model were measured simultaneously in two turbulent boundary layers, which simulated the natural winds over typical open country and urban terrains; the length scale of these flows ranged from 1/400 to 1/500. These flows are referred to as Flows 'I' and 'II', respectively. The span (diameter) D of the wind tunnel models was 267 mm, which corresponded to approximately 100 to 130 m in full scale. The span to height ratio D/H ranged from 1 to 5.33. The wind pressures at all taps were sampled at a rate of 1000 samples per second on each channel for a period of approximately 33 seconds. The compensation for the frequency response of the pressure measurement system was carried out by using a digital filter, which was designed so that the dynamic data up to approximately 500 Hz could be obtained without attenuation and distortion. All measurements were made at a wind speed of 10 m/s at a reference height of $z_{ref} = 267$ mm. The details of the experimental apparatus and procedures are presented in Hongo (1995). From the simultaneous pressure measurements, the modal forces $F_i(t)$ for the first 11 modes are computed. Each asymmetric mode ($m \neq 0$) has its counterpart with the same natural frequency and a vibration mode that is the same in shape but rotated about the center (see Table 1). Such a mode is also considered here. The modal force is reduced to a coefficient $C_{Fi}(t)$ defined as follows :

$$C_{Fi}(t) = \frac{F_i(t)}{q_H \cdot B_i} \quad (1)$$

where q_H = dynamic pressure of the flow at the roof height H ; and B_i is defined by the following equation :

$$B_i = \int_0^{D/2} \int_0^{2\pi} \phi_i^2(r, \theta) r dr d\theta \quad (2)$$

The time history of the modal force coefficients is used for the dynamic response analysis of roofs (Section 4.1).

The second series of wind tunnel experiments (series 'B') aimed at obtaining data for the first

Table 2 Experimental conditions: α = power law exponent of the mean wind speed profile; U_H, I_{uH} = mean wind speed and turbulence intensity of the flow at the model height H .

Series	Measurement	Model			Flow		
		D (mm)	H (mm)	No.	α	U_H (m/s)	I_{uH} (%)
A	Point pressures at 433 points	267	50.1 - 267	I	0.15	7.6 - 10	18.2 - 13.6
				II	0.24	6.4 - 9.8	26.5 - 15.5
B	First modal force	160 - 220	30	I*	0.15	10	15.8
				II*	0.27	8.9	24.6
		80 - 220	40	I*	0.15	10	15.4
				II*	0.27	8.9	23.1

modal force under various conditions. The results are used for constructing an empirical formula for the gust effect factor (Section 5.2); the data of the series ‘A’ experiments are also used for this purpose. The experiments were carried out in an Eiffel-type wind tunnel with a working section of 6.5 m in length and 1.0×1.4 m in cross-section at Tohoku University. The pressure measurements were made in two turbulent boundary layers, Flows ‘I*’ and ‘II*’, which approximately corresponded to the above mentioned Flows ‘I’ and ‘II’, respectively. The length scale of these flows was approximately 1/500. The height of the models was 30 or 40 mm and the D/H ratio was varied from 2 to 7.3. In order to measure the first modal force, a pneumatic averaging technique was used; regarding this technique, see Davenport and Surry (1984), and Uematsu *et al.* (1996, 1997b). The number of pressure taps ranged from 64 to 128, depending on the model’s diameter. Small restrictor tubes were used to attenuate peaks in the frequency response of the tubing. The amplitude response of the measurement system was within 5% of unity up to approximately 100 Hz. Therefore, no correction was applied to the results. The signal from the transducer was sampled at a rate of 1000 samples per second for a period of 30 seconds.

4. Dynamic response of circular roofs

4.1. Method of analysis

A modal analysis in the time domain is applied to the evaluation of the dynamic response of a roof with $D = 50 - 150$ m; nineteen modes, i.e., three axisymmetric and eight pairs of asymmetric modes, are used (see Table 1). The effect of the internal pressure is not considered. The wind speed U_H at the roof height H is varied from 25 to 60 m/s, depending on the roof height. The modal displacement $a_i(t)$ is computed by numerically integrating the equation of motion for $a_i(t)$, using the Newmark β method with $\beta = 1/4$. The structural damping η_i is assumed 0.02 for all modes. The time step Δt for the numerical integration is 0.005 s, which is approximately 1/200 of the first natural period $T_1 = 1/f_1$. Since the time step for the wind loads is much longer than Δt , the Spline functions of the third order are applied to the discrete values of $C_{Fi}(t)$ obtained from the Series ‘A’ experiments, in order to obtain the intermediate values. The lateral displacement w of the roof is computed by superimposing the responses in all modes considered. Furthermore, the resultant bending moment M is computed based on a thin plate theory. We focus on the distributions of w and M at a moment when these values become the maxima, w_{\max} and M_{\max} , during a period of 600 seconds.

4.2. Results and discussion

Computations were made for 60 cases with different values of D , D/H , U_H , etc. Fig. 4 shows sample results on the distributions of w , positive downward, and M along the center line parallel to the wind direction at a moment when the maximum responses, w_{\max} and M_{\max} , are observed during a period of 600 seconds ($D = 100$ m, Flow I, $U_H = 40$ m/s); w and M are reduced by using D and D_b . In the figure, x represents the distance from the leading edge. Each broken line stands for the result of a run of computation. As might be expected, the results are scattered to some degree. The negative value of w over the whole roof area indicates that the roof deforms upward, and the maximum deflection w_{\max} is observed near the center. On the other hand, the maximum bending moment M_{\max} occurs at $x \approx D/6$.

Fig. 5 shows the contribution of each mode to w_{\max} and M_{\max} for $D/H = 5.33$ by triangles. It is

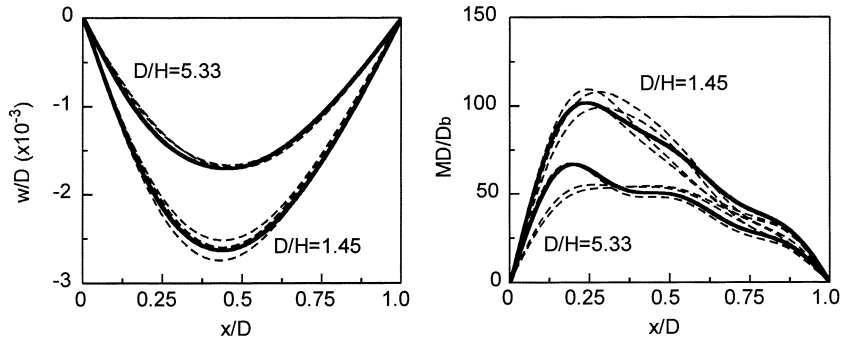


Fig. 4 Distributions of deflection w and bending moment M along the center line parallel to the wind direction: $D = 100$ m, Flow I, $U_H = 40$ m/s

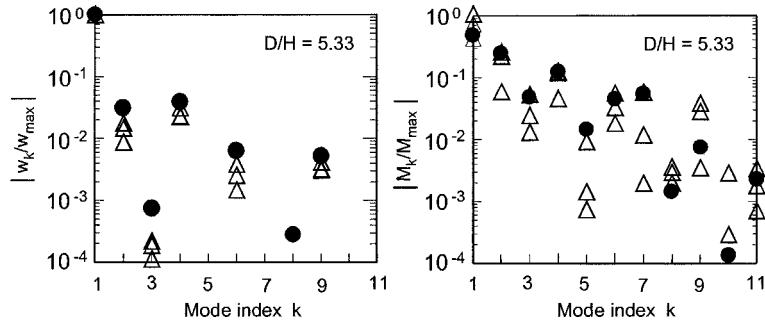


Fig. 5 Contribution of each mode to the maximum response: $D = 100$ m, $D/H = 5.33$, Flow I, $U_H = 40$ m/s

found that the deflection is dominated by the first mode (axisymmetric mode); the contribution of the other mode to w_{\max} is less than 0.5 percent. On the other hand, the bending moment is influenced by several modes; besides the first mode, the contribution of the second (the first asymmetric) and the fourth (the second asymmetric) mode is relatively great. These features were generally observed for other cases.

5. Evaluation of design wind loads for structural frames

5.1. Application of gust effect factor approach

As mentioned above, we can compute the dynamic response of the roof accurately by using the time history of wind pressures at many points on the roof. However, this procedure is somewhat complicated and time consuming. By comparison, if we can evaluate the maximum load effect, or the design wind load, based on the gust effect factor approach, it may be quite useful from the practical point of view. Considering the fact that the roof's response is generally dominated by the first mode, we may consider only this mode for evaluating the gust effect factor for the purpose of simplicity; in other words, the gust effect factor for the first mode is applied to the other modes also. The gust effect factor G_f may be given by the following equations :

$$G_f = 1 + g \cdot r_F \cdot R \quad (3)$$

$$g \approx \sqrt{2 \ln 600 f_1} + \frac{0.577}{\sqrt{2 \ln 600 f_1}} \quad (4)$$

$$r_F = \frac{C'_{F1}}{|\bar{C}_{F1}|} \quad (5)$$

$$R = \left(1 + \frac{\pi}{4 \eta_1} \frac{f_1 \cdot S_{F1}(f_1)}{\sigma_{F1}^2} \right)^{1/2} \quad (6)$$

where g = peak factor; \bar{C}_{F1} and C'_{F1} stand for the mean and rms values of the first modal force coefficient $C_{F1}(t)$; R = resonant magnification factor; σ_{F1} = standard deviation of the first modal force $F_1(t)$; and $S_{F1}(f)$ represents the power spectrum of $F_1(t)$. The effects of the turbulence intensity of the approach flow and the building geometry on the roof's dynamic response are included in the evaluation of r_F and $f_1 S_{F1}(f_1) / \sigma_{F1}^2$. The maximum response may be given by the product of the mean response and the gust effect factor G_f . The deflection \tilde{w} and the resultant bending moment \tilde{M} due to the equivalent static load, given by the product of the time-averaged wind pressure and G_f , can be computed by the following equations :

$$\tilde{w} = G_f \sum_k \bar{w}_k = G_f \sum_k \bar{a}_k \phi_k(r, \theta) \quad (7)$$

$$\tilde{M} = -D_b \left\{ \nabla^2 \tilde{w} - (1 - \nu) \left(\frac{1}{r} \frac{\partial \tilde{w}}{\partial r} + \frac{1}{r^2} \frac{\partial^2 \tilde{w}}{\partial \theta^2} \right) \right\} \quad (8)$$

where \bar{a}_k = time-averaged k -th modal displacement; and ν represents an equivalent Poisson's ratio for the roof structure, when represented by a thin elastic plate.

The distributions of \tilde{w} and \tilde{M} along the centerline parallel to the wind direction, which are predicted by the above mentioned gust effect factor approach, are represented by the thick solid lines in Fig. 4 and by the closed circles in Fig. 5. A good agreement is seen between the time history analysis and the gust effect factor approach for the deflection. On the other hand, the distribution of bending moment predicted by the gust effect factor approach is somewhat different in shape from that of the time history analysis. However, the gust effect factor approach almost captures the maximum value obtained from the time history analysis in any case. Similar comparison was made for all cases. Figs. 6(a) and 6(b) show histograms of the ratio of the result from the time history analysis to that predicted by the gust effect factor approach for w_{\max} and M_{\max} , respectively. The figure includes the results obtained under various conditions; the total number of data is 242. The mean and the standard deviation of the data are respectively 1.01 and 0.081 for w_{\max} , and 0.96 and 0.11 for M_{\max} . A good agreement between these two results is observed, which suggests that the gust effect factor approach can be applied to the evaluation of the design wind loads for the flat roofs under consideration; this may be the case for other configurations, such as rectangular, for example.

5.2. Empirical formula for gust effect factor

According to Eq. (3), we can easily compute G_f , if we know the values of r_F and the reduced power spectrum $f S_{F1}(f) / \sigma_{F1}^2$ of $F_1(t)$ at $f=f_1$. These values are strongly affected by the behavior of the separated shear layer from the windward edge of the roof and therefore they depend on the

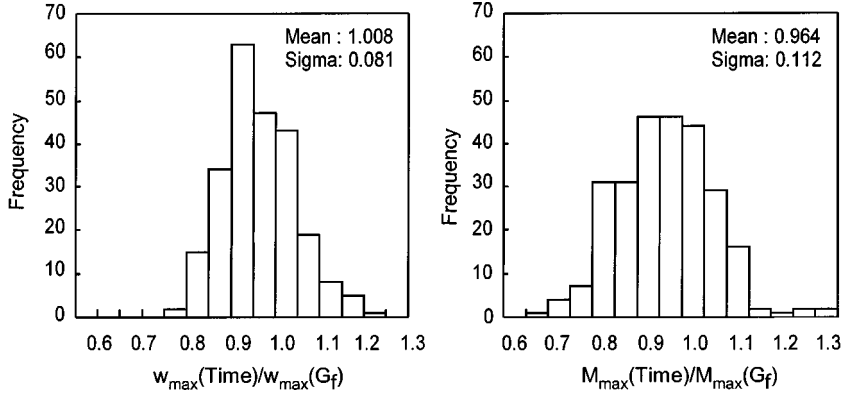


Fig. 6 Comparison between time history analysis and gust effect factor approach for the maximum deflection w_{\max} and the maximum bending moment M_{\max}

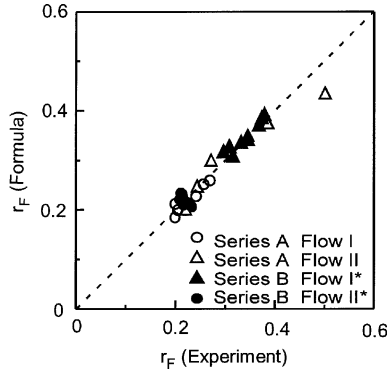


Fig. 7 Comparison between formula and experiment for r_F

building geometry (i.e., D and H) and the turbulence intensity I_{uH} of the approach flow at the roof height. The dependence of r_F and $f S_{F_1}(f) / \sigma_{F_1}^2$ on these parameters was investigated, based on the experimental results for $F_1(t)$.

The empirical formula for r_F we obtained is as follows :

$$r_F = 3.4 I_{uH}^2 \cdot \exp\left(0.04 \frac{D}{H}\right) + 0.12 \quad (9)$$

Fig. 7 shows a comparison between formula and experiment for r_F ; in the figure, the results for all cases tested in the present study are plotted. The discrepancy between both results is within approximately $\pm 10\%$.

The reduced power spectra $f \cdot S_{F_1}(f) / \sigma_{F_1}^2$ of $F_1(t)$ for various cases are plotted against a reduced frequency f^* ($=f\sqrt{DH}/U_H$) in Fig. 8; \sqrt{DH} is used as a representative length for reducing the frequency, because the spectrum seems to be dependent on both D and H . Note that we used H as a representative length for Beam type roofs and rectangular roofs of Plate type in our previous studies (Uematsu *et al.* 1997a,b). The general shape of the reduced power spectrum within the whole frequency range depends on the roof geometry as well as on the flow characteristics. However, the effect of these factors is not so great, in particular, for a relatively high reduced-frequency range,

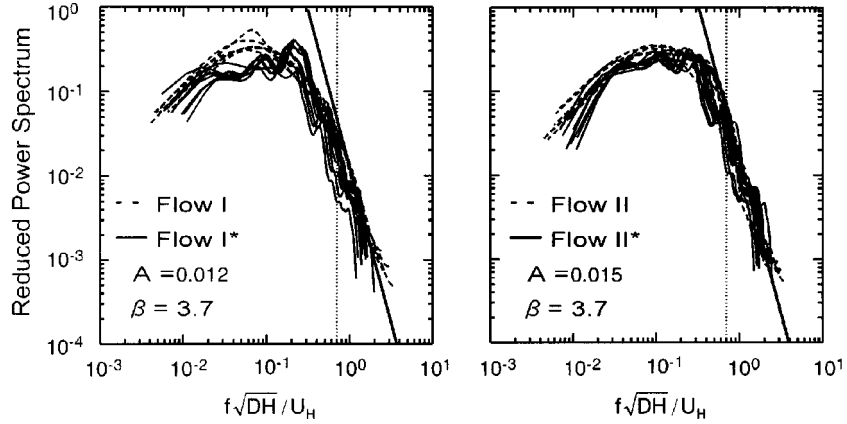


Fig. 8 Reduce power spectrum $f S_{F_1}(f) / \sigma_{F_1}^2$ of the first modal force $F_1(t)$

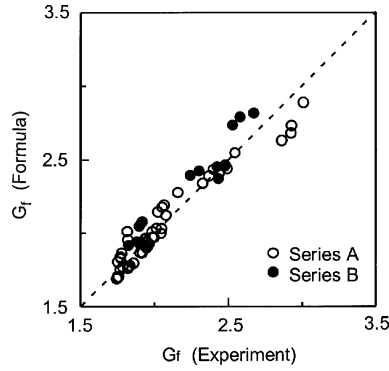


Fig. 9 Comparison between formula and experiment for G_f

such as $f^* > 0.7$, for example, which is often important for evaluating the resonant effect under practical conditions. As was done in our previous studies, the reduced power spectrum in a reduced-frequency range $f^* > 0.7$ can be approximated by the following equation:

$$\frac{f \cdot S_{F_1}(f)}{\sigma_{F_1}^2} = A \cdot \left(\frac{f \sqrt{DH}}{U_H} \right)^{-\beta} \quad (10)$$

The parameters A and β are determined so that the above equation fits well the experimental results for $f^* > 0.7$. The thick solid line in Fig. 8 represents the empirical equation, fitted by eye. The value of β is almost the same for all flows. On the other hand, the value of A is somewhat dependent on the flow turbulence. It is found that the value of A increases slightly with an increase in I_{uH} . A similar trend was observed for rectangular flat roofs (see Uematsu *et al.* 1997b). Although there is a deviation of the experimental results from the empirical equation, it is not a serious problem for predicting G_f , because G_f is not so sensitive to the degree of approximation for the reduced power spectrum.

Using the above equations (Eqs. 3-6, 9 and 10), we can compute G_f quite easily. To investigate the validity of the formula, we made a comparison for G_f between the predicted values by the formula and those computed by using the experimental results for the first modal force directly. The results are plotted in Fig. 9. The agreement is generally good; the formula can predict the value of G_f with an error less

than approximately $\pm 10\%$. The result confirms the validity of the formula obtained in this study.

5.3. Equivalent design pressure coefficient

The equivalent pressure coefficients, which reproduce the maximum load effects, are investigated. As is often used in the building codes, the distribution of the mean pressure coefficient C_p is represented as shown in Fig. 10. That is, the roof is divided into a windward high-suction area ($0 \leq x \leq \xi$) and a downstream low-suction area ($\xi \leq x \leq D$), and the pressure coefficient (C_{p1} or C_{p2}) in each area is assumed constant. The values of C_{p1} and C_{p2} are given by averaging the C_p -distribution along the centerline over $0 \leq x \leq \xi$ and $\xi \leq x \leq D$, respectively. The value of ξ is determined so that the equivalent pressure coefficients, when combined with the above mentioned gust effect factor G_f , gives the same value of w_{\max} (or M_{\max}) that was obtained from the time history analysis. The results of a preliminary analysis indicated that the values of C_{p1} and C_{p2} for the optimum ξ value depend slightly both on the flow characteristics and on the roof geometry. Therefore, we set $C_{p1} = -1.0$ and $C_{p2} = -0.12$, as representative values for these two areas. A comparison between experiment and model for the C_p -distribution is presented in Fig. 11. Plotted in Fig. 12 are the values of ξ , determined from w_{\max} and M_{\max} , against H/D . The data for various conditions approximately collapse onto a curve given by the following equation :

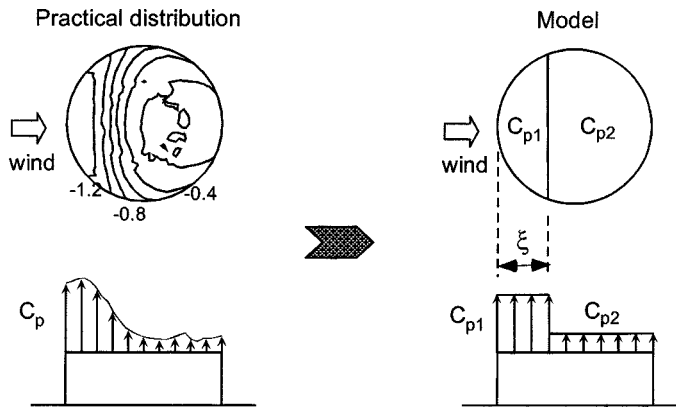


Fig. 10 Model of pressure coefficient distribution on the roof

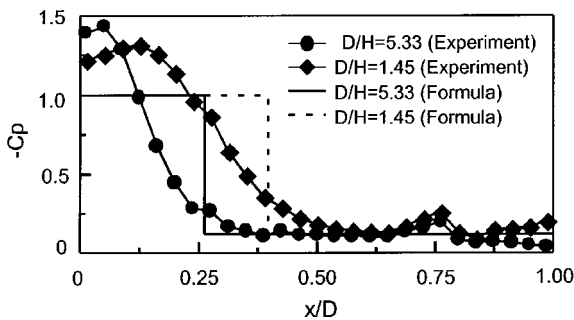


Fig. 11 Comparison between experiment and model for C_p -distribution along the centerline of the roof

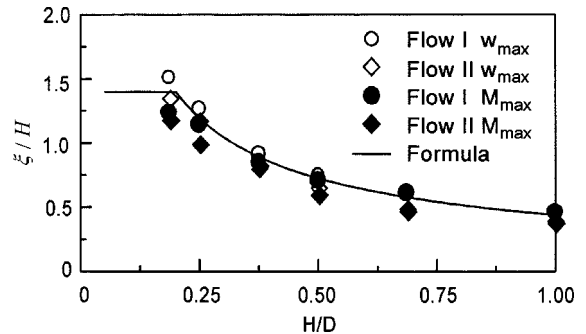


Fig. 12 Plots of ξ/H as a function of H/D

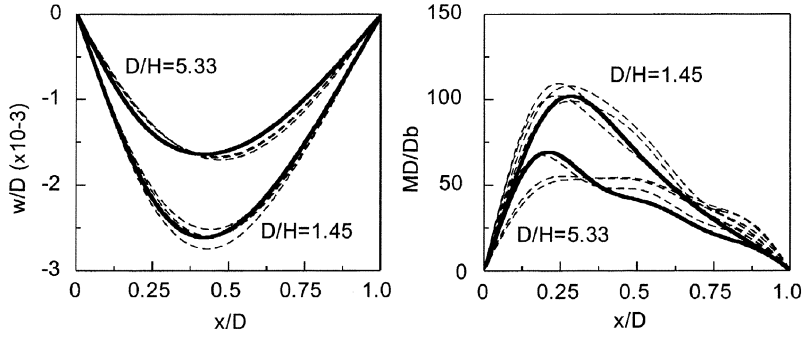


Fig. 13 Comparison between time history analysis and prediction by the formula for the distributions of deflection w and bending moment M along the center line parallel to the wind direction: $D = 100$ m, Flow I, $U_H = 40$ m/s

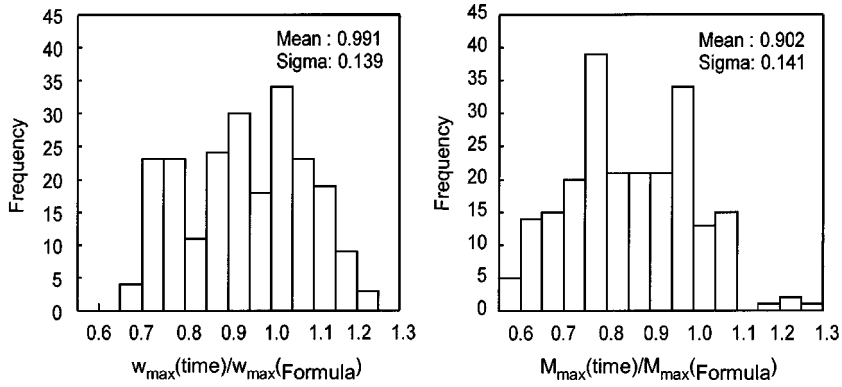


Fig. 14 Comparison between time history analysis and prediction by the formulas for the maximum deflection w_{\max} and the maximum bending moment M_{\max}

$$\frac{\xi}{H} = 0.44 \left(\frac{H}{D} \right)^{-0.72} \quad \text{for} \quad 0.2 \leq \frac{H}{D} \leq 1 \quad (11a)$$

$$\frac{\xi}{H} = 1.4 \quad \text{for} \quad \frac{H}{D} < 0.2 \quad (11b)$$

Eq. (11b) should be regarded as tentative, because there are not sufficient data for $H/D < 0.2$. However, it may be reasonable to assume that the value of ξ/H becomes almost independent of D in this range of H/D , because the pressure field near the leading edge is primarily affected by H and, therefore, ξ is proportional to H .

Using Eqs. (3), (4), (9), (10) and (11), together with the above-mentioned values of C_{p1} and C_{p2} , we can compute the equivalent pressure coefficient distribution, which may be used for the structural design of circular flat roofs. To investigate the application of the formulas, we compared the distributions of w and M due the equivalent static pressure with those obtained from the time history analysis. The results corresponding to Fig. 4 are shown in Fig. 13. It is found that the results predicted by the formula (thick solid lines) agree reasonably well with those obtained from the time history analysis (broken lines). Furthermore, a comparison was made for the values of w_{\max} and M_{\max} . Fig. 14 shows histograms of the ratio of the result from the time history analysis to that

predicted by the formulas for w_{\max} and M_{\max} ; the number of data is 242. The mean and the standard deviation of the data are respectively 0.99 and 0.14 for w_{\max} and 0.90 and 0.14 for M_{\max} . It can be seen that the agreement between these two results is relatively good, although the empirical formulas are very simple. Therefore, the formulas can be applied to the evaluation of the design wind pressure in the structural design of circular flat roofs.

6. Conclusions

The wind-induced dynamic response of circular flat roofs with long spans has been studied. The results suggest that a gust effect factor approach, in which only the first mode is considered for evaluating the gust effect factor G_f , can be applied to the evaluation of the design wind loads for the structural frames of these roofs. An empirical formula for G_f and the equivalent pressure coefficients to be used for the structural design was provided. Using these formulas, we can easily compute the design wind loads, within an allowable error. Further investigations are planned to improve upon the formulas so that they can yield more accurate estimations of the design wind loads for a wide range of building shapes and structural systems.

Acknowledgements

The authors would like to thank Mr. A. Sasaki, a former graduate student of Tohoku University, for help with the wind tunnel experiments and data processing. Acknowledgement also is due to Dr. T. Hongo of Kajima Technical Research Institute for many valuable discussions.

References

- Davenport, A.G. and Surry, D. (1984), "Turbulent wind forces on a large span roof and their representation by equivalent static loads", *Canadian J. of Civ. Eng.*, **11**, 955-966.
- Hongo, T. "Experimental study of wind forces on spherical roofs", Ph.D. Thesis, Tohoku University, 1995 (in Japanese).
- Marukawa, H., Uematsu, Y., Tamura, Y., Nakamura, O. and Ueda, H. (1993), "Design wind loads on flat long-span roof", *Proc. the 4th East Asia-Pacific Conf. on Struct. Eng. and Construct.*, Seoul, Korea, 1619-1624.
- Sasaki, A., Uematsu, Y., Yamada, M. and Hongo, T. (1999), "Wind-induced dynamic response and its load estimation of circular flat roofs with long spans", *J. Struct. Construct. Eng.*, AIJ, **517**, 39-44 (in Japanese).
- Ueda, H. and Tamura, Y. (1994), "Equivalent design pressure coefficients for beams supporting flat roofs", *J. Struct. Construct. Eng.*, Architectural Institute of Japan, **464**, 59-69 (in Japanese).
- Uematsu, Y., Yamada, M. and Sasaki, A. (1996), "Wind-induced dynamic response and resultant load estimation for a flat long-span roof", *J. Wind Eng. Ind. Aerod.*, **65**, 155-166.
- Uematsu, Y., Yamada, M. and Karasu, A. (1997a), "Design wind loads for structural frames of flat long-span roofs: Gust loading factor for the beams supporting roofs", *J. Wind Eng. Ind. Aerod.*, **66**, 35-50.
- Uematsu, Y., Yamada, M. and Karasu, A. (1997b), "Design wind loads for structural frames of flat long-span roofs: Gust loading factor for a structurally integrated type", *J. Wind Eng. Ind. Aerod.*, **66**, 155-168.
- Uematsu, Y., Yamada, M., Sasaki, A. and Hongo, T. (1998), "Design wind loads for structural frames of circular flat roofs", *Proc. of the 2nd East European Conf. on Wind Eng.*, Prague, Czech Republic, 525-532.